H_2-O_2 SUPERCRITICAL COMBUSTION MODELING USING A CFD CODE

by

Abdallah BENAROUS and Abdelkrim LIAZID

Original scientific paper
UDC: 662.769.2:629.7
DOI: 10.2298/TSCI0903139B

The characteristics of propellant injection, mixing, and combustion have a profound effect on liquid rocket engine performance. The necessity of raising rocket engines performance requires a combustion chamber operation often in a supercritical regime. A supercritical combustion model based on a one-phase multi-components approach is developed and tested on a non-premixed H_2-O_2 flame configuration. A two equations turbulence model is used for describing the jet dynamics where a limited Pope correction is added to account for the oxidant spreading rate. Transport properties of the mixture are calculated using extended high pressure forms of the mixing rules. An equilibrium chemistry scheme is adopted in this combustion case, with both algebraic and stochastic expressions for the chemistry/turbulence coupling. The model was incorporated into a computational fluid dynamics commercial code (Fluent 6.2.16). The validity of the present model was investigated by comparing predictions of temperature, species mass fractions, recirculation zones and visible flame length to the experimental data measured on the Mascotte test rig. The results were confronted also with advanced code simulations. It appears that the agreement between the results was fairly good in the chamber regions situated downstream the near injection zone.

Key words: *non-premixed combustion, H_2-O_2 flame, supercritical pressure, transport properties, Mascotte test rig*

Introduction

Chemical propulsion has been the mainstay of space exploration propulsion since the beginning of space missions, it's still the only technology applicable to launch from earth to space with a higher payload to cost ratio [1]. In this context, the use of liquid propellant engines provides good flexibility and better performance, this type of engines can be designed to be throttled and fired more than once in each mission.

The use of cryogenic propellants in liquid rocket engines (LRE) at chamber pressures that exceed critical point of the mixture has been well established as a combination that provides high efficiency and performance for a variety of launch vehicle applications. In particular, liquid oxygen-hydrogen (LOX-H_2) engines have been developed for a variety of launch systems, including the space shuttle mean engine (SSME) and the Ariane5 Vulcain engine.

To accurately predict the performances and the internal thermal environment of the engine using computational fluid dynamics (CFD) methods, the degree of local mixing and the extent of the combustion reactions must be established. The involved processes of injection, mixing and combustion have a decisive influence on rocket engine performance, combustion stability, and service lifetime [2].

Although LOX-H_2 rocket engines have been operating relatively safely for the past several years, the processes that control combustion are still not well understood [3]. Today, some very detailed investigations of these processes are available. There are studies on the evaporation, mixing, and combustion of liquid or supercritical droplets in a quiescent or moving gaseous surrounding [4-7] and supercritical shear flows as occurring at the coaxial injection into the rocket combustors by direct numerical simulations (DNS) [8, 9], and large eddy simulations (LES) [9-10]. These detailed investigations are very important for the understanding of the complex mixing and combustion processes occurring in rocket combustion chambers, but nowadays, these methods are still too computationally expensive to use them for industrial applications. Here still Reynolds averaged Navier-Stockes (RANS) methods are applied to support the design process. Two of the latest publications based on a RANS method for the description of a supercritical combustion using commercial CFD-codes are Poschner *et al*. [11] which used ANSYS-CFX for a diffusion H_2-O_2 turbulent flame and Minotti *et al.* [12] for CH_4-O_2 systems using Fluent software.

The aim of this work is to implement a homogeneous multi-component one phase model in the Fluent 6.2.16 [13] material database and to carry out a faithful description of the H_2-O_2 supercritical combustion with a less computational cost. The model treats liquids-gas mixture as coexisting continua and assumes there is no thermal or velocity lag between phases. This avoids modeling drop size and calculating droplet trajectories. The model is based on an accurate representation of the viscosity and thermal conductivity of the H_2/O_2 mixture and use a polynomial fits of the temperature for describing the density and thermodynamic properties. Emphasis is placed on shear-coaxial injection processes in the laboratory-scale uni-element rocket configuration (Mascotte) developed at ONERA in Châtillon, France. On this test rig, the data were deemed to be the benchmark test cases for multiphase spray flows presented by the 2nd International workshop on rocket combustion modeling (IWRCM) committee [14].

Phenomenological trends

Shear coaxial injection processes in LRE exhibit two distinct modes of combustion [15]. At sub-critical pressures, the liquid jets atomize, here, dynamic forces and surface tension promote the formation of heterogeneous spray and lifted spray flames form in a manner consistent with the modes of combustion exhibited by local drop clusters. When chamber pressures approach or exceed the critical pressure of a particular propellant, the injected liquid jet undergo a transcritical change of state as interfacial temperatures rise above the critical temperature of the local mixture. For this situation, diminished inter-molecular forces promote diffusion dominated mixing processes prior to atomization [16].

Above the mixture critical point, liquid and gaseous phases are no longer separated. Indeed, the recent flow visualizations [15] confirm that the surface and surface tension of the oxygen liquid core vanish, the sharp distinction between gas and liquid disappears and the entire field essentially becomes a continuous medium with no abrupt phase change involved in the burning process. Small changes of state lead to huge gradients in density and thermodynamic variables during the mixing and make the accurate prediction of the processes taking place very difficult [9].

Governing equations

The reacting flow equations of mass, momentum, total energy and chemical species are written, respectively, in conservative forms as:

$$\frac{\partial \rho}{\partial t} \quad \vec{} \quad (\rho \vec{\mathrm{u}}) \quad 0 \tag{1}$$

$$\rho \frac{\partial \vec{\mathrm{u}}}{\partial t} \quad \rho \vec{\mathrm{u}} (\vec{} \quad \vec{\mathrm{u}}) \quad \vec{} p \quad \vec{} \boldsymbol{\tau} \tag{2}$$

where

$$\boldsymbol{\tau} \quad \frac{2}{3} \mu (\vec{} \quad \vec{\mathrm{u}}) \boldsymbol{I} \quad \mu (\vec{} \quad \vec{\mathrm{u}} \quad \vec{} {}^{t} \vec{\mathrm{u}}) \tag{3}$$

τ and $\boldsymbol{I}$ denote the viscous stress and the identity tensors, respectively, and μ is the molecular dynamic viscosity;

$$\rho \frac{\partial e}{\partial t} \quad \rho \vec{\mathrm{u}} \quad \vec{} e \quad p \vec{} \quad \vec{\mathrm{u}} \quad \boldsymbol{\tau} \quad \vec{} \quad \vec{\mathrm{u}} \quad \vec{} \quad \vec{\mathrm{q}} \tag{4}$$

where e and $\vec{\mathrm{q}}$ are the specific internal energy and the total heat fluxes, respectively. When neglecting molecular diffusion caused by temperature gradient (Soret effect) and thermal diffusion caused by a concentration gradient (Dufour effect), the heat flux can be expressed as:

$$\vec{\mathrm{q}} \quad \lambda \vec{} T \quad \underset{\alpha}{} \rho D_{\alpha} h_{\alpha} \vec{} Y_{\alpha} \tag{5}$$

where

$$h_{\alpha} \quad \int_{T^0}^{T} c p_{\alpha} \mathrm{d}T \quad h_{\alpha,F} \tag{6}$$

is the partial enthalpy of the i^{th} species in the mixture;

$$\rho \frac{\partial Y_{\alpha}}{\partial t} \quad \rho \vec{\mathrm{u}} \quad \vec{} Y_{\alpha} \quad \vec{} \quad (\rho D_{\alpha} \vec{} Y_{\alpha}) \quad \varpi_{\alpha} \tag{7}$$

ϖ_{α} represents the instantaneous rate of production of the i^{th} chemical species due to reactions.

Heat release due to chemical reactions in the energy equation is accounted for in description of the partial specific enthalpies h_{α} by including the enthalpy of formation $h_{\alpha,\mathrm{F}}$ in its definition. Radiation fluxes and body forces are currently neglected.

In the case of supercritical combustion regimes, assuming the gas mixture having an ideal behavior leads to large errors up to 650% in predicting the fields of temperature and species mass fractions [17]. Hence, the density is deemed as a function of pressure and temperature as:

$$\rho = \rho(T, p) \tag{8}$$

For most turbulent combustion calculations, it is not possible to solve the previous system of equations directly. Averaged forms are mandatory to access the mean quantities of the flow unknowns. Every extensive quantity φ (except density and pressure), can be decomposed into a mean part $\widetilde{\varphi}$ and a fluctuating part φ" as:

$$\varphi \quad \widetilde{\varphi} \quad \varphi \tag{9}$$

where the Favre (mass weighted) averaging form is defined as:

$$\widetilde{\varphi} \quad \frac{\overline{\rho \varphi}}{\overline{\rho}} \tag{10}$$

The averaging leads generally to unclosed terms in the momentum, species transport, and energy equations, which are modeled using the eddy viscosity, dissipation, and diffusivity hypothesis, respectively, as:

$$\overline{\rho u_i u_j} \quad \mu_t \frac{\partial \widetilde{u}_i}{\partial x_j} \quad \frac{\partial \widetilde{u}_j}{\partial x_i} \quad \frac{2\delta_{ij}}{3} \frac{\partial \widetilde{u}_k}{\partial x_k} \tag{11}$$

$$\overline{\rho u_j Y_\alpha} \quad \frac{\mu_t}{\mathrm{Sc}_t} \frac{\partial \widetilde{Y}_\alpha}{\partial x_j} \tag{12}$$

$$\overline{\rho u_j h} \quad \frac{\mu_t}{\mathrm{Pr}_t} \frac{\partial \widetilde{h}}{\partial x_j} \tag{13}$$

where $\mathrm{Sc_t}$ and $\mathrm{Pr_t}$ are the turbulent Schmidt and Prandtl numbers supposed identical to treat turbulent diffusion processes for heat and species identically. The system of equations can be closed by choosing a model for the turbulent viscosity μ_t. This is done in this paper by a simple *k-ε* turbulence model, solving two additional transport equations for the turbulent kinetic energy *k* and its dissipation rate ε. The turbulent viscosity is modeled as:

$$\mu_t \quad C_\mu \rho \frac{k^2}{\varepsilon} \tag{14}$$

Properties evaluation

Above the critical point, molecular transport properties exhibit anomalous behavior and are extremely sensitive to both local temperature and pressure. This is due to a transition of molecular ordering or to small-scale circulation effects resulting from the migration of clusters of molecules. Hence, terms relating to mixture dynamic viscosity – μ, in eq.(3), thermal conductivity – λ, in eq. (5), and the species diffusion coefficient in the mixture – D_α, in eq.(7), have a considerable contribution on the mixing process [5].

Kinematic diffusivity

In Fluent, diffusion coefficient is calculated by default from the bulk mass diffusivity available in its material database. Because here, the mixing is diffusion controlled process, the assumption of constant diffusivities may lead to large errors. Hence, diffusion coefficient of a species α in the mixture at a reference pressure p^0 can be calculated using the Blanc's law :

$$D_\alpha^0 \quad \frac{1}{\sum_{\beta \neq \alpha} \frac{Y_\beta}{D_{\alpha\beta}}} \tag{15}$$

where $D_{\alpha\beta}$ is the binary diffusion coefficient evaluated via the relation derived from the Chapman-Enskog theory [18]:

$$D_{\alpha\beta}^0 \quad \frac{0.0143 \sqrt[4]{T^3}}{p M_{\alpha\beta} (\sqrt[3]{C_\alpha} \quad \sqrt[3]{C_\beta})^2} \tag{16}$$

with

$$M_{\alpha\beta} \quad \frac{2 M_\alpha M_\beta}{M_\alpha \quad M_\beta} \tag{17}$$

and $\mathrm{M_\alpha}$ and $\mathrm{M_\beta}$ are the molecular weights of components α and β and C_α and C_β are their atomic diffusion volumes, respectively. The extension of the previous relations to high pressures is made by the correlation of Takahashi [19]:

$$D_{\alpha\beta} \quad D^{0}_{\alpha\beta} \frac{p^{(0)}}{p} H(1 \quad A \ T_r^{\ B})(1 \quad GT_r^{\ E}) \tag{18}$$

and $T_r = T/T_c$ where T_c is the critical temperature of the mixture which is lower than the critical temperature of the pure oxygen, and A, B, E, G, and H are empirical coefficients.

Molecular (dynamic) viscosity

In Fluent, molecular viscosity of a mixture can be evaluated by a volume weighted or a mass weighted mixing laws, which do not account for molecular interactions at high pressure.

For polyatomic molecular gases like hydrogen and oxygen, we use a method proposed by Chung *et al*. [20] containing a potential energy term Ω^* which describes the interaction between molecules:

$$\mu \quad (4.0785 \ 10^{-5}) \frac{\sqrt{MT_c}}{\Omega^* \sqrt[3]{V_c^2}} F_c \tag{19}$$

$$F_c = F_c(w, \mu d, T_c) \tag{20}$$

The dynamic viscosity is a function of the mixture critical point (T_c, V_c), the collision parameter (Ω^*), the Pitzer's acentric factor w and the dipole moment μd which are a self characteristics of the molecule's shape. At a particular pressure, the molar critical volume V_c and the collision parameter Ω^* are tabulated for various reduced temperatures [21].

Thermal conductivity

An extension of the Eucken model [22] for the thermal conductivity of dilute gases was proposed by Chung *et al.* [21] as:

$$\lambda \quad \mu \frac{7.452}{M} \Psi(w, T_r, cv) \tag{21}$$

Specific heat capacity at constant volume is also evaluated at each prescribed pressure as a function of the reduced temperature.

Mixture density

At high pressures and low temperatures, the equation of state (EOS) for the mixture differs significantly from that of the ideal gas equation. The choice of the EOS based on the Pen-Robinson (PR) formulation is a result of a comparison between the relations of Lee-Kesler, Soave, and Redlich-Kwong made in the work developed by Harstad *et al.* [23]. This equation is a three parameter formula accounting additionally for the deviation of molecule from spherical shape. It has the following expression:

$$p \quad \frac{RT}{V \quad b} \quad \frac{a\alpha(T)}{V^2 \quad 2bV \quad b^2} \tag{22}$$

with

$$a = a(T_c, p_c) \text{ and } b = b(T_c, p_c) \tag{23}$$

and

$$\alpha(T) \quad [1 \quad \delta(1 \quad \sqrt{T_r})]^2 \quad \text{with} \quad \delta \quad \delta(w) \tag{24}$$

The coefficients *a*, *b*, and *w* are relating to the mixture, and are obtained from those of individual species using recent mixing rules [24]. In this paper, we use the data [21] obtained from the PR EOS for the H_2-O_2 mixture for a prescribed pressure as a piecewise polynomial of the temperature.

Configuration and operating conditions

The present study concerns a subscale thrust chamber of the Mascotte single injector test case RCM-3 (Rocket Combustion Modeling, Version 3) [4]. The high pressure combustion chamber is a cylindrical duct of 50 mm inner diameter and a 400 mm length (fig. 1). At its downstream end is a nozzle of variable shape having a convergent length of 20 mm and a throat diameter of 9 mm allowing a chamber pressure of about 60 bar, however, because of the lack of experimental data about the nozzle flow, this last was not included in the 2-D axisymmetrical model (fig. 2).

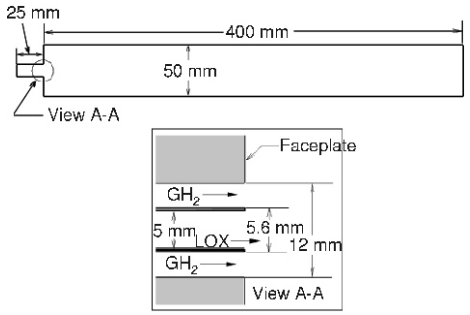

Figure 1. Configuration of the RCM-3 test case

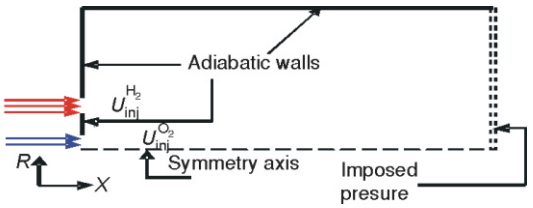

Figure 2. Geometrical modeling and boundary conditions

Table 1. Operating conditions for RCM-3 test case

Operating conditions	H_2	O_2
Pressure [bar]	60	60
Temperature [K]	287	100
Mass flow rate [kgs^{-1}]	0.070	0.100
Injector inlet velocity [ms^{-1}]	236	4.35

This version of the test rig in use since 1997 allows operating conditions (until 100 bar) above the critical pressure of oxygen (50.4 bar).The operating conditions used for the present simulation are summarized in tab. 1.

A preliminary simulation of the injector inflow for each propellant was carried out [25] in order to get the velocity profile for an established turbulence at the injector exit. This last, will be used as a velocity inlet condition for the combustion chamber, and one will be able to proceed to a geometrical shrinking of the injectors (fig. 2). At the outlet, a pressure of 60 bar was prescribed and the walls of the chamber were assumed to be smooth and adiabatic.

Chemistry and turbulence modeling

The chemistry model used in simulation is of great importance for predicting the temperature field. As it was confirmed in the works of Cheng *et al*. [26, 27], the equilibrium chemistry and chemical kinetic are almost identical because the H_2-O_2 reactions are extremely fast at high pressure conditions. The minor effect of rate chemistry can only be seen at the region very close to the injector tip where the flow's residence time is extremely short.

A preliminary thermo-chemical work [25] was done using the rocket module of the CEA (Chemical Equilibrium and Applications) Fortran code [28] on the H_2/O_2 combustion under RCM-3 conditions. The analysis shows that the dominant combustion products were restricted to four species (H_2O, OH, O, H) with a particular dominance of the OH radical over dissociation products. This result is completely identical to kinetic chemistry analyses made at ONERA [29]. Hence, the use of a complete reaction model without considering the hydroxyl radical will probably not be suitable for this situation.

In the non-premixed combustion cases, the algebraic approaches are mainly based on the work of Magnussen *et al*. [30]. In this context, the eddy dissipation model (EDM) supposes that the chemical reactions are fully controlled by the turbulent mixing which tends to bring back the fuel and the oxidant to a reaction zone where the large eddies occurs.

Chemical kinetics effects are not considered in the reaction rate calculation. This makes the model well suitable for one step global reaction. To account for OH radical, we also use a stochastic approach based on a conserved scalar. Here, a transport equation for this scalar (mixture fraction) is solved and individual component concentrations are derived from the predicted mixture fraction distribution using the prePDF module [13]. Turbulence-chemistry coupling effects are accounted for with help of a presumed probability density function (PDF) which is supposed to have a Beta shape.

Keeping in mind that the standard k-ε model overestimates mixing and turbulence levels of axisymmetrical jets [27], a Pope correction is added to the kinetic energy dissipation rate equation [31]. This last is corrected by adding a production term which takes into account of vortex stretching effect on the jet viscosity and consequently on its spreading rate:

$$\frac{\partial}{\partial x_j}(\overline{\rho}\widetilde{u}_j\widetilde{\varepsilon}) \quad \frac{\partial}{\partial x_j}\frac{\mu_t}{\sigma_\varepsilon}\frac{\partial\widetilde{\varepsilon}}{\partial x_j} \quad \frac{\widetilde{\varepsilon}}{\widetilde{k}}(C_{1\varepsilon}P_K \quad \overline{\rho}C_{2\varepsilon}\widetilde{\varepsilon} \quad \overline{\rho}C_{3\varepsilon}\chi\widetilde{\varepsilon}) \tag{25}$$

where

$$P_{\mathrm{K}} \quad \overline{\rho u_i u_j}\frac{\partial\widetilde{u}_i}{\partial x_j} \tag{26}$$

is the production rate of the turbulence energy and

$$\chi \quad \omega_{ij}\omega_{ji}S_{li} \quad \text{where} \quad \omega_{jl} \quad \frac{1}{2}\frac{\widetilde{k}}{\widetilde{e}}\frac{\partial\widetilde{u}_j}{\partial x_l} \quad \frac{\partial\widetilde{u}_j}{\partial x_l} \quad \text{and} \quad S_{li} \quad \frac{1}{2}\frac{\widetilde{k}}{\widetilde{\varepsilon}}\frac{\partial\widetilde{u}_j}{\partial x_l} \quad \frac{\partial\widetilde{u}_j}{\partial x_l} \tag{27}$$

Here χ denote the invariant vortex stretching and $C_{3\varepsilon}$ is a strictly positive Pope constant. The correction is practically done by choosing an appropriate value for the new turbulence constant appearing in eq. (25).

$$C_{2\varepsilon} \quad C_{2\varepsilon} \quad \chi C_{3\varepsilon} \tag{28}$$

Results and discussions

The first step in carrying out the flame simulation is to set up the geometric mesh. It is developed by implementing throughout the entire axisymmetrical domain a quadrilateral elements scheme while keeping

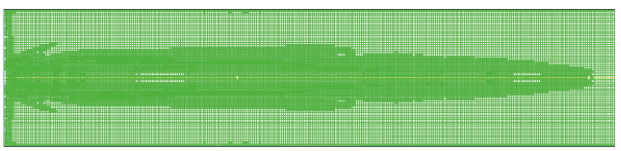

Figure 3. Grid refinement zone

the element size at 60 μm [26], hence, a primary structured mesh containing 28256 quadrilateral elements, was created.

In order to improve the results quality in the zones of strong gradients, an adaptive mesh refinement (AMR) technique was adopted. The algorithm adaptively creates finer grids depending on where in the domain extra solution is needed according to a user defined error estimator. In the present work, the axial velocity gradient (imposed at 3%) was chosen as an estimation quantity, on a basis of which, a grid refinement will occur. The initial simulations show a strong velocity gradient in a mixing layer zone situated along the potential core.

Consequently, refinement was located at this zone and the local grid spacing was reduced to 35 μm. The resulting mesh containing 30306 elements was retained for the simulations.

Cold flow simulation

The propellant flow in each injector was analyzed separately and a fully developed turbulence was ensured at their exit sections. The corresponding velocity profiles [25] were used to initialize the flow in the chamber and allow us to keep the injector's flow history. In the absence of chemical reactions, the species transport equation is solved without considering the production source term; the corresponding simulation is called cold flow. It is particularly interesting because it separates the effect of turbulent mixing from combustion such that, one can validate the appropriate turbulence model for the hot fire simulation.

In order to get a better approach to the flow behavior predicted by Villermaux's theory [32], a Pope correction was made by adjusting turbulence constant from the default value $C_{2\varepsilon}$ = = 1.92 to a value that gives a maximum half jet spreading $C_{2\varepsilon}$ = 1.89 when maintaining a fixed value of $C_{1\varepsilon}$ = 1.44. The half jet spreading is defined here as arctangent of the line that fits the locus of points where O_2 mass fraction is 90%.

The contour of the axial velocity (fig. 4) shows clearly a corner recirculation zone which is due to the presence of the wall, and an oxidant-front recirculation zone which extends downstream of the mixing layer and considered as a consequence of the shearing between the propellant flows.

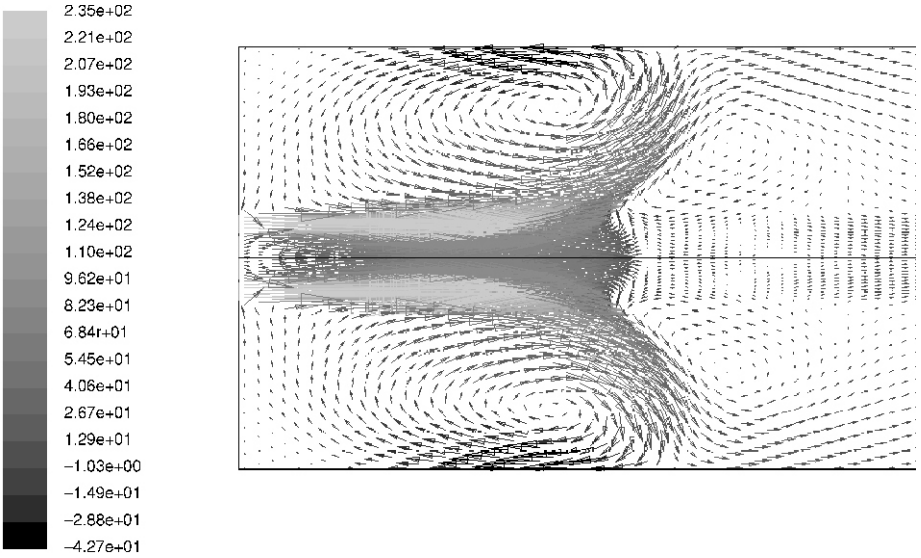

Figure 4. Contour of the axial velocity

Because of the high value of the chamber to oxidant injector diameter ratio (about 10) and due to the high turbulence intensity of the fuel stream, the recirculation zones affect also the species distribution and consequently the local mixing. Indeed, radial profile of the oxygen mass fraction at a near (X = 10 mm) and a far (X = 250 mm) stations from the faceplate, present a quasi asymptotic behavior which shows the existence of a zone where the oxygen is trapped (figs. 5a and b).

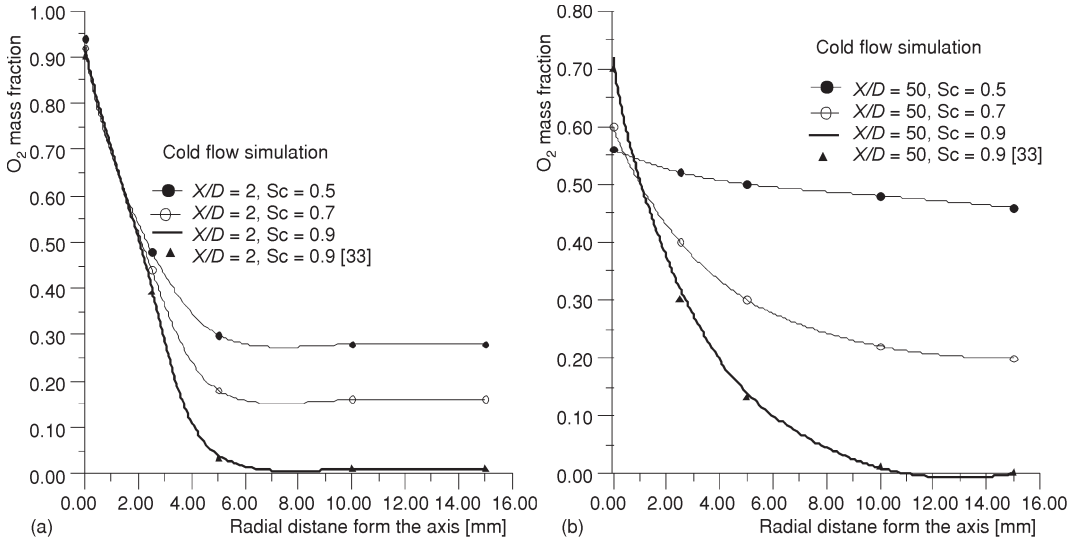

Figure 5. Oxygen mass fraction near (a) and far (b) from the injector

As hydrogen is much more diffusive substance than water vapor and oxygen, the mixing process as estimated using a standard (or bulk) viscosity for calculating kinematic diffusivity might be misrepresented and the region of pure oxygen persists slightly far the downstream than using the mixing rule of the Takahashi correlation approach [19].

It is also important to note that effect of turbulent diffusion characterized by the turbulent Schmidt number on the fresh mixture quality is significant far away from the injector (fig. 5b).

The oxygen mass fraction decreases averagely of 98% when changing the Schmidt number value from Sc_t = 0.5 (high hydrogen diffusivity) to Sc_t = 0.9 (default value on the ONERA CEDRE code). Nevertheless, the diffusion influence is not so important near the injector face (fig. 5a) and becomes insignificant when one approaches the centerline of the chamber. This behavior is quite similar to results obtained in cold flow experimentations [33].

Hot fire simulation

In the EDM model, every reaction has the same turbulent rate which is inversely proportional to the large-eddy mixing time scale (k/ε) [30]. Using this model in a multi-step reaction mechanism will likely produce incorrect solution, because the Arrhenius rates differ for each reaction. A single step chemistry model with the complete following reaction:

$$H_2 + (1/2)O_2 \quad H_2O$$

gives much too high temperature that exceeds 4200 K (fig. 6) compared to the adiabatic flame temperature value (AFT =3615 K, fig. 7) predicted by the rocket module of CEA [28].

Comparing with the experimental data [14], an overestimation of 400 K is noted on the peak value of the axial static temperature when neglecting dissociation products. Taking into account for additionally species (H, O, OH, H_2O_2), the maximum temperature (fig. 8) resulting from applying the flamelet model was found about 3200 K which is more realistic value, but the real temperature is still underestimated [11].

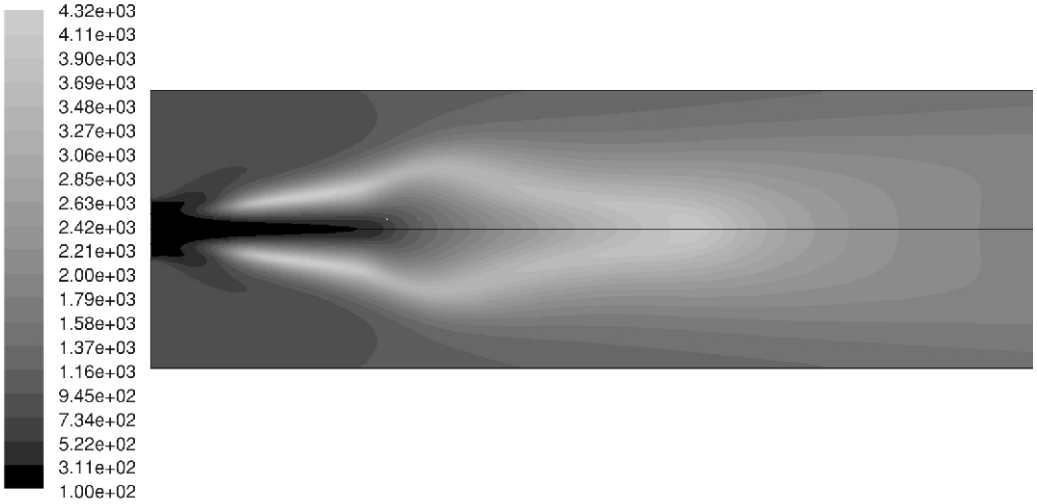

Figure 6. Temperature distribution (EDM model)

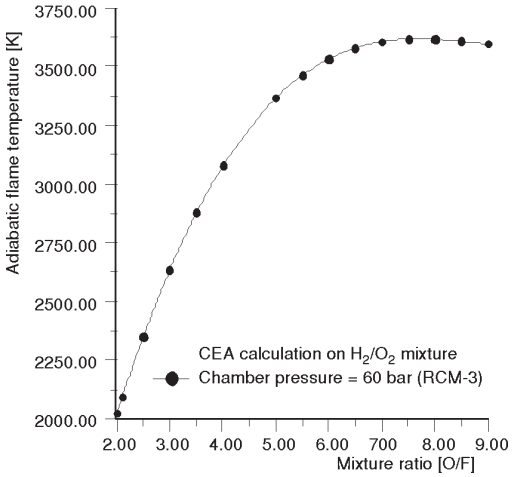

Figure 7. Adiabatic flame temperature for various mixture ratio

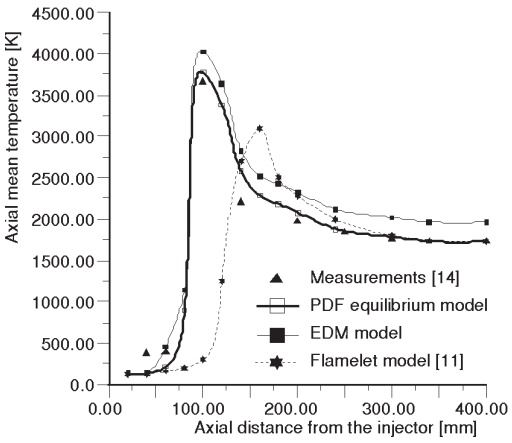

Figure 8. Axial temperature profiles for various chemistry models

In a second step, we use an equilibrium Beta-pdf approach containing the same type and number of species (H_2, O_2, H_2O, OH, O, H) as it was found in CEA analysis and ONERA scramjets studies [29]. Look-up tables of temperature, density, and species mass fractions for

various mean mixture fraction (and its variance) are created in a PDF file, which can be read by the Fluent solver. Here we do not need to define the reaction mechanisms and, instead, the system is treated using chemical equilibrium calculations. This approach seems to be well adapted for H_2-O_2 single coaxial injection and combustion since the flame temperature was over predicted about 2.2% only (fig. 8).

Comparing the axial temperature distribution of the flame resulting from EDM and PDF models, it can be recognized that position of maximum temperature (fig. 8) indicating the flame tip, is located at about the same axial location (100 mm) for both combustion models, but it is slightly downstream when using a flamelet model.

It is also noted that the axial static temperature at various radial positions shows a decrease of the peak value and a retreat of its position (fig. 9) compared with the centerline profile (R/D = 0) when exploring the flow radial direction. The estimated profile is quite similar to those obtained by using a mature home-made code [26]. This can be explained by a well prediction of the jet spreading angle.

Using the stochastic model, the OH mass fraction at an axial position (fig.10) is quite similar to the results obtained by applying advanced real fluid models [26]. A slight disparity of 15% on the hydroxyl mass fraction is noted near the faceplate, but becomes weak far downstream of the injection zone. Unfortunately, there are not OH distribution data to validate our numerical results at various radial positions. Because of the smaller and wider range of turbulent and chemistry scales (non-equilibrium effects) in the near injection zone and due to a non-fully supercritical regime, it is of importance to account for mass and heat transfer lag between surrounding gas and the small amounts of residual dispersed phase. These are the causes for which the results of the model deviate slightly from the experimental data in this region.

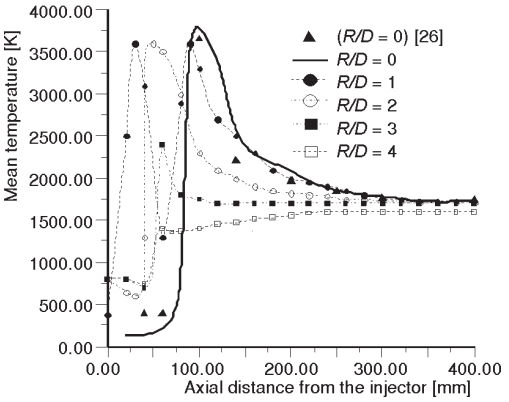

Figure 9. Temperature profiles at different radial locations

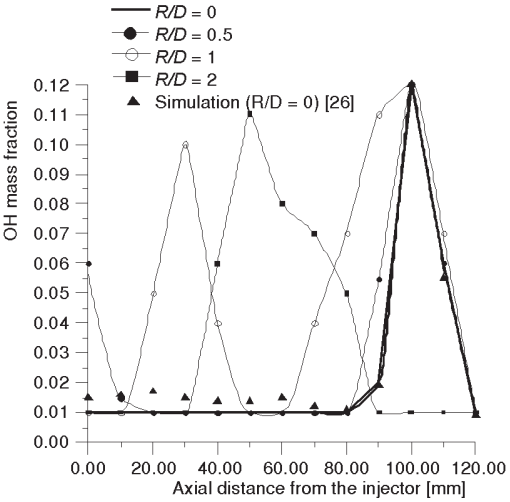

Figure 10. OH mass fraction for various radial positions

Conclusions

In this paper, supercritical H_2-O_2 combustion is investigated using an improved mixing model. The results are validated by using the test bench Mascotte RCM-3 case.

The single one-step EDM yields temperatures up to 4200 K, which are much higher than the AFT (3615K) predicted by the rocket module of the NASA-CEA Fortran code. More-

over, the flamelet model containing additional species provides reasonable maximum temperature (3200 K) which is however, even lower than the experimental data.

Including an equilibrium Beta-PDF chemistry description, the temperature was overestimated by 2.2% only. An attempt to fit simulation results with experiments by modifying turbulence constants was performed. Indeed, since it is known from literature that for axisymmetric free jets, the k-ε overestimates the turbulent kinetic energy, a Pope correction was added to the dissipation rate equation. A modification of the $C_{2\varepsilon}$ constant to 1.89 provided a qualitative prediction of the spreading angle and the visible flame length.

Numerical simulation of the H_2-O_2 supercritical combustion with the one phase multi-component model exhibits good agreements qualitatively; detailed experimental data will provide further model validation in the future works.

Nomenclature

$C_{1\varepsilon}$, $C_{2\varepsilon}$, $C_{3\varepsilon}$, C_μ – turbulence model constants
C_α – atomic diffusion volume of a component, [Ks^3kg^2m]
cp, cv – specific heat capacity at constant pressure (volume), [$JkgK^{-1}$]
D – diameter, [m]
D_α, $D_{\alpha\beta}$ – mixture diffusion, binary diffusion coefficient, [m^2s^{-1}]
e – internal energy, [Jkg^{-1}]
h_α – enthalpy of the component, [Jkg^{-1}]
k – turbulent kinetic energy, [m^2s^{-2}]
$\boldsymbol{I}$ – identity tensor
M – molecular weight, [$gmol^{-1}$]
P_K – production rate of turbulent kinetic energy, [$kgms^{-3}$]
Pr – Prandtl number
p – static pressure, [Pa]
$\vec{q}$ – heat flux, [Wm^{-2}]
R – radial position, [m]
Sc – Schmidt number
S_{ij} – rate of strain, tensor
T – temperature, [K]
$\vec{u}$, u_i – velocity vector, i^{th} component, [ms^{-1}]
V – molar volume, [m^3mol^{-1}]
w – Pitzer's acentric factor
x_i, X – i^{th} Cartesian coordinate, axial position, [m]
Y_α – mass fraction of a component α

Greek symbols

ε – dissipation rate of k, [m^2s^{-3}]
λ – thermal conductivity, [$Wm^{-1}K^{-1}$]
μ – dynamic viscosity, [$kgm^{-1}s^{-1}$]
ϖ_α – net production rate of a component, [kgm^3s^{-1}]
ω_{ij} – rotation tensor
ρ – density, [kgm^{-3}]
σ_ε – turbulence model constant
τ – viscous stress tensor
χ – vortex stretching invariant

Subcripts

c – critical
F – formation
r – reduced
t – turbulent
$\bar{}$ – Reynolds averaging
$\sim$ – Favre averaging
" – fluctuation

References

[1] Stevenson, J. D., Cheap Access to Space and Minimum Cost Design, Lecture Series No.11, Massachusetts Institute of Technology, Cambridge, Mass., USA, 2002
[2] Haidn, O. J., Habiballah, M., Research on High Pressure Cryogenic Combustion, *Aerospace Science and Technology, 7* (2003), 6, pp. 473-491
[3] Oefelein, J. C., Thermophysical Characteristics of Shear-Coaxial LOX-H_2 Flames at Supercritical Pressure, *Proceeding of the Combustion Institute*, Pittsburgh, Penn., USA, 2005, pp. 2929-2937
[4] Miller, R. S., Harstad, G., Bellan, J., Evaluation of Equilibrium and Non Equilibrium Evaporation Models for Many Droplet Gas-Liquid Flow Simulations, *International Journal of Multiphase Flow, 24* (1998), 6, pp. 1025-1055

[5] Yang, V., Modeling of Supercritical Vaporization, Mixing and Combustion Processes in Liquid- Fueled Propulsion Systems, *Proceedings of the Combustion Institute,* Pittsburgh, Penn., USA, 2000, pp. 925-942
[6] Delplanque, J. P., Sirignano, W., Numerical Study of Transient Vaporization of an Oxygen Droplet at Sub- and Super-Critical Conditions, *International Journal of Heat and Mass Transfer, 36* (1993), 2, pp. 303-314
[7] Daou, J., Haldenwang, P., Nicoli, C., Supercritical Burning of Liquid Oxygen (LOX) Droplet with Detailed Chemistry, *Combustion and Flame, 101* (1995), 1-2, pp. 153-169
[8] Miller, R. S., Harstad, G., Bellan, J., Direct Numerical Simulations of Supercritical Fluid Mixing Layers Applied to Heptane-Nitrogen, *Journal of Fluid Mechanics, 436* (2001), 6, pp. 1-39
[9] Oefelein, J. C., Mixing and Combustion of Cryogenic Oxygen-Hydrogen Shear Coaxial Jet Flames at Supercritical Pressure, *Combustion Science and Technology, 178* (2006), 1-3, pp. 229-252
[10] Zong, N., Yang, V., Cryogenic Fluid Jets and Mixing Layers in Transcritical and Supercritical Environments, *Combustion Science and Technology, 178* (2006), 1-3, pp.193-227
[11] Poschner, M. M., Pfitzner, M., Real Gas CFD Simulation of Supercritical H_2-LOX Combustion in the Mascotte Single-Injector Combustor using a Commercial CFD Code, AIAA paper 2008-952, 2008
[12] Minotti, A., Bruno, C., Comparison between Real and Ideal Sub and Supercritical Combustion Simulations of LO_2-CH_4 LRE Flames at 15 MPa, 46th AIAA Aerospace Science and Meeting, Reno, NV, USA, 2008
[13] ***, Fluent Software, Ver.6.2.16, Lebanon, N. H., USA, 2005
[14] Thomas, J. L., Zurbach, S., Test Case RCM3: Supercritical Spray Combustion at 60 bars at Mascotte, *Proceeding*, 2nd International Workshop on Rocket Combustion Modeling, Lampoldhausen, Germany, 2001, pp. 13-23
[15] Mayer, M., Tamura, H., Propellant Injection in a Liquid Oxygen/Gaseous Hydrogen Rocket Engine, *Journal of Propulsion and Power, 12* (1996), 6, pp. 1137-1147
[16] Juniper, M., *et al*., The Structure of Cryogenic Flames at Elevated Pressure, *Proceeding of the Combustion Institute*, Pittsburgh, Penn., USA, 2000, Vol. 1, pp. 1103-1109
[17] Minotti, A., Bruno, C., Sub-Trans and Supercritical Properties for LO_2-CH_4 at 15 MPa, *Journal of Thermophysics and Heat Transfer, 21* (2007), 4, pp. 796-810
[18] Chapman, S., Cowling, T. G., The Mathematical Theory of Nonuniform Gases, Cambrigde University Press, London, 1952
[19] Takahashi, S., Preparation of a Generalized Chart for the Diffusion Coefficients of Gases at High Pressures, *Journal of Chemical Engineering in Japan, 7* (1974), 6, pp. 417-420
[20] Chung, T. H., *et al*., Generalized Multiparameter Correlation for Non Polar Fluid Transport Properties, *Industrial and Engineering Chemistry Research, 27* (1988), 4, pp. 671-679
[21] Lemmon, E. W., McLinden, M. O., Friend, D. G., Thermophysical Properties of Fluid Systems, NIST Chemistry WebBook, 2005, http://webbook.nist.gov/
[22] Svehla, R. A., Estimated Viscosities and Thermal Conductivities of Gases at High Temperatures, Report No. 132, Lewis Research Center, 1962, Cleveland, O., USA
[23] Harstad, K. G., Miller, R. S., Bellan, J., Efficient High Pressure State Equations, *AIChE Journal, 43* (1997), 6, pp. 1605-1610
[24] Adachi, Y., Sugie, H., A New Mixing Rule- Modified Conventional Mixing Rule, *Fluid Phase Equilibria, 28* (1986), 2, pp. 103-118
[25] Benarous, A., Liazid, A., Karmed, D., H_2/O_2 Combustion under Supercritical Conditions, *Proceeding*, 3rd European Combustion Meeting, Creete, Greece, 2007, pp. 156-161
[26] Cheng, G., Farmer, R., Real Fluid Modeling of Multiphase Flows in Liquid Rocket Engine Combustors, *Journal of Propulsion and Power, 22* (2006), 6, pp. 1373-1381
[27] Cheng, G., Farmer, R., Development of Efficient Real Fluid Model in Simulating Liquid Rocket Injector Flows, AIAA paper 2003-4466, 2003
[28] Gordon, S., McBride, B. J., Computer Program for Calculation of Complex Chemical Equilibrium Compositions and Applications, NASA Reference Publication No.1311, Lewis Research Center, Cleveland, O., USA, 1994
[29] Gaffie, D., *et al*., Numerical Investigation of Supersonic Reacting Hydrogen Jets in a Hot Air Co-flow, AIAA paper 01-1864, 2001
[30] Magnussen, B. F., Hjertager, B. H., On Mathematical Models of Turbulent Combustion with Special Emphasis on Soot Formation and Combustion, *Proceedings*, 16th International Symposium on Combustion, The Combustion Institute, Pittsburgh, Penn., USA, 1976, pp. 719-729

[31] Pope, S. B., An Explanation of the Turbulent Round-Jet/Plane-Jet Anomaly, *AIAA Journal, 16* (1978), 3, pp. 279-281
[32] Villermaux, E., Mixing and Spray Formation in Coaxial Jets, *Journal of Propulsion and Power, 14* (1998), 5, pp. 807-817
[33] Schmidt, V., *et al*., Experimental Investigation and Modeling of the Ignition Transient of a Coaxial H_2/O_2 Injector, *Proceeding*, 5th International Symposium on Space Propulsion, Chattanooga, Tenn., USA, 2003, pp. 8-36

Authors' affiliations:

A. Benarous (**corresponding author**)
Laboratoire de Combustion et Détonique (LCD)
UPR 9028 CNRS
Université de Poitiers – ENSMA
BP 40109 , Téléport 2
1, Avenue Clément Ader
F-86961 Futuroscope Chasseneuil Cedex, France
Département de Mécanique
Université Hassiba Benbouali de Chlef, BP 151
02000 Chlef, Algeria
E-mail: benarous@ensma.fr, abenarous@yahoo.fr

A. Liazid
Laboratoire de Recherche en Technologie de l'Environnement (LTE)
Ecole Nationale Supérieure de l'Enseignement Technique d'Oran (ENSET),
BP 1523, 31000 Oran, Algérie

Paper submitted: November 15, 2008
Paper revised: February 4, 2009
Pape accepted: March 4, 2009